JACS
JOURNAL OF THE AMERICAN CHEMICAL SOCIETY

Article

pubs.acs.org/JACS

Dendritic and Nanowire Assemblies of Condensed DNA Polymer Brushes

Dan Bracha and Roy H. Bar-Ziv*

Department of Materials and Interfaces, The Weizmann Institute of Science, Rehovot 76100, Israel

Supporting Information

ABSTRACT: We investigated the collective conformational response of DNA polymer brushes to condensation induced by the trivalent cation spermidine. DNA brushes, a few kilobase-pairs long, undergo a striking transition into macroscopic domains of collapsed chains with fractal dendritic morphology. Condensation is initiated by focal nucleation of a towerlike bundle, which laterally expands in a chain-reaction cascade of structural chain-to-chain collapse onto the surface. The transition exhibits the hallmarks of a first-order phase transition with grain boundaries, hysteresis, and coexistence between condensed and uncondensed phases. We found that an extended DNA conformation is maintained throughout the transition and is a prerequisite for the formation of large-scale dendritic domains. We identified a critical DNA density above which the nucleation propensity and growth rate sharply increase. We hypothesize that the ability of DNA-scaffolding proteins to modify the local DNA density within a genome may act as a dynamic and sensitive mechanism for spatial regulation of DNA transactions in vivo by selective condensation of chromosomal territories. By assembling a DNA brush along a patterned line narrower than twice the DNA contour length and tuning the local surface densities, we were able to initiate nucleation at a predefined location and induced growth of a single condensed nanowire over a distance 2 orders of magnitude longer than the single-chain contour. Our results demonstrate spatial control of condensation as a new tool for constructing DNA-based synthetic systems with important implications for regulation of DNA transactions on surfaces.

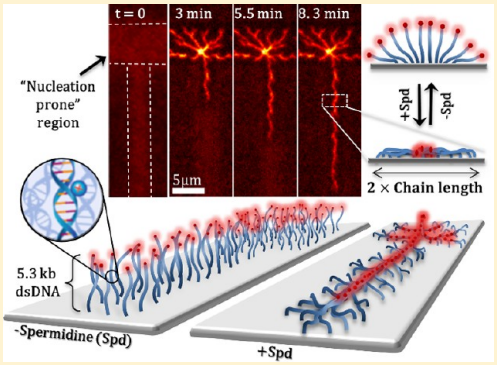

INTRODUCTION

The remarkable ability of DNA to collapse into a compacted form is essential for genome organization,[1,2] protection,[3,4] and regulation[5−7] and bears important implications for gene delivery[8] and synthetic biology.[9−11] In vivo, the transition is facilitated by specialized proteins, macromolecular crowding, and multivalent polyamines, where in some cases the last of these play the dominant role.[12−14] Mechanistically, polyamines such as spermidine^{3+} (Spd) exchange low-valence counterions in neutralizing the DNA[15,16] while mediating DNA−DNA attraction through charge-correlation interactions.[17] Beyond a critical Spd concentration, DNA segments locally align at interhelix distances of 2.9 nm[18] by a reversible first-order phase transition that follows nucleation and growth.[16,19,20] At low DNA density in vitro, Spd-induced condensates typically assume a toroidal shape,[21] which is dictated by the balance between the surface energy of the condensate and the chain bending rigidity.[22] At high density on the other hand, freely diffusing DNA chains tend to aggregate into multimolecular liquid-crystalline phases with cholesteric or columnar hexagonal order.[18,23] Although similar symmetries have been observed in vivo, the overall morphology of genomic DNA condensates has a much higher level of complexity[2,13] involving (i) the coexistence of condensed regions that are inaccessible to DNA transaction machinery and uncondensed regions that are biochemically active[24,25] and (ii) a network of dynamic structural constraints of loops, bends, and cross-links via chromatin architecture proteins, which by themselves do not induce condensation in vitro yet provide internal scaffolding with nonuniform spatial density to the DNA phase. Applying such structural constraints on precondensed chains in vitro has been shown to affect the structural characteristics of the condensate,[26,27] suggesting that condensation may be responsive to DNA architecture in vivo. So far, however, the roles of local DNA density, internal organization, and spatial segregation in affecting condensation initiation, regulation, and morphology remain poorly understood. Acquiring the ability to design condensate shape and to obtain coexistence in vitro could open new possibilities for the development of novel DNA-based nanomaterials as well as for spatial regulation of gene expression in synthetic systems.

DNA brushes consisting of a few kilobase-pair (kb) chains packed on a biochip at a cellular-like density of ∼10^7 base pairs (bp)/μm^3 (10 mg/mL) recently emerged as a model system simulating the crowded, segregated, and constrained environment of genomic DNA.[28−30] The considerable overlap of closely patterned chains has been shown to induce collective phenomena that do not appear in dilute solution.[28,31−33] Direct brush-height measurements revealed a collective transition

Received: October 27, 2013
Published: March 5, 2014

 © 2014 American Chemical Society dx.doi.org/10.1021/ja410960w | J. Am. Chem. Soc. 2014, 136, 4945−4953

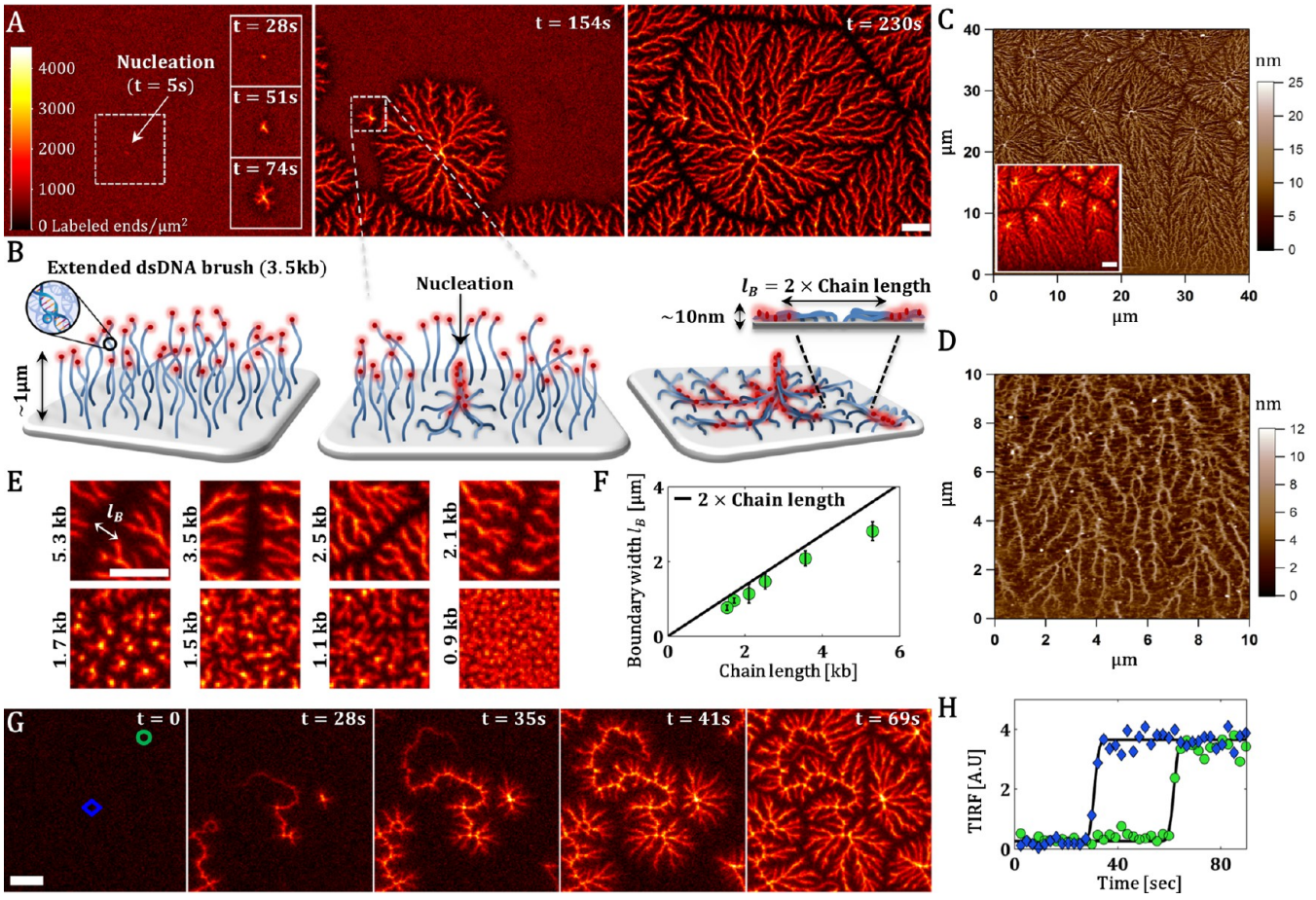

Figure 1. Dendritic assemblies of condensed DNA. (A) Fluorescence images (time in seconds from Spd addition) of a uniform 3.5 kb DNA brush undergoing condensation via nucleation and growth into dendritic domains (Movie S1). The DNA free ends were fluorescently labeled, and the intensity color code indicates the local fluorophore density due to two dimensional displacement of free ends. Sharp interdomain boundaries appear at fluorophore-depleted regions, with the overall fluorescence intensity remaining fixed (Figure S2A). (B) Schematic representation of the structural transition. (C) Wet AFM scan confirming the dendritic structure observed by fluorescence (inset) and indicating collapse of the extended brush (~1um in height) to a height of no more than 25 nm above surface. (D) Wet AFM scan showing branching of the structure into bundles of locally aligned chains. (E) Fluorescence images showing that the width of the boundary between domains increases with chain length (Figure S4). (F) Plot showing that the boundary width corresponds to twice the contour length (dashed line), indicating fully extended chain collapse. (G) Dynamics of brush height revealed by TIRF microscopy (Movie S2). The appearance of fluorescence marks the collapse of the ~1 μm stretched chains to a height at which the labeled free ends are deep within the evanescent excitation length (~100 nm; Figure S2B), showing radial and single-extension growth modes. (H) Plots of TIRF intensity as a function of time for early-condensing (blue diamonds) and late-condensing (green circles) regions, indicating that the chains remain extended right until they sharply collapse. Scale bars are 5 μm.

from a relaxed coil to a full-contour-length stretch that follows a universal polyelectrolyte brush scaling of density to ionic strength ratio for mono- and divalent salts,[31] enabling accurate control of the DNA conformation in the dense phase. Perturbing dense layers of relaxed chains using Spd was recently shown to induce a coil-to-globule transition,[34] yet the roles of interchain distance, local density, chain length, and conformation were not addressed.

In this work, we investigated Spd-induced transitions in a dense DNA brush in response to variations in the structural properties of the precondensed phase by monitoring height changes and lateral organization of tethered 0.9−5.3 kb chains using real-time fluorescence microscopy, evanescent microscopy, and wet atomic force microscopy (AFM). We report on the collapse of extended DNA brushes into stable and ordered dendritic domains with lateral dimensions of tens of micrometers and well-defined nuclei and grain boundaries. We found that the collective DNA conformation determines the condensate morphology and that an extended brush conformation is a prerequisite for large-scale dendritic structures. The molecular chain configuration was revealed, as well as two distinct growth modes in which chains maintain their extended form throughout the transition. We identified a critical DNA density for condensation above which the nucleation lag time decreases and the growth rate increases. Hysteresis was observed in the reversible condensation cycle, on which basis we were able to stabilize the coexistence of condensates and a brush phase that can be spatially controlled through variations in local DNA density. Finally, by controlling the timing and location of nucleation while restricting the available area for growth, we were able to demonstrate the formation of guided nanowires of coaligned chains along a distance of tens of micrometers.

RESULTS

Nucleation and Growth of Condensed DNA in a Brush. A uniform 3.5 kb DNA brush with its free 5′ ends fluorescently labeled was assembled on a glass surface coated

dx.doi.org/10.1021/ja410960w | J. Am. Chem. Soc. 2014, 136, 4945−4953

with a biocompatible layer using a photochemical approach.[30] The surface density was estimated as ~550 chains/μm^2 (14 ± 2 fluorophores/pixel), corresponding to a mean interchain distance of ~40 nm.[29] The brush was immersed in a low-salt solution (3 mM NaCl), an osmotic brush regime in which the osmotic pressure due to the confined ions induces maximal swelling of the brush up to the 1.2 μm chain contour length.[31] The Spd concentration (C_{Spd}) was incrementally increased by adding minute volumes of concentrated Spd solution to the reservoir. Passing 60 μM Spd initiated a major change in the surface fluorescence, which began with the emergence of a single bright spot surrounded by a ~1 μm thick perimeter with reduced fluorescence (Figure 1A and Movie S1 in the Supporting Information). The fluorescence intensity at the center saturated at a value nearly 10-fold greater than that for the mean fluorophore density of the unperturbed brush. This nucleation event was followed by a process of lateral growth via radially forming dendritic-like extensions as the uniform brush developed into a continuously branching domain with a fractal dimension of 1.75 (Figure S1 in the Supporting Information). Over time, new nucleation centers emerged and grew. When fronts of adjacent domains met, a well-defined boundary with nearly no fluorescence signal formed, eventually leading to the conversion of the entire brush into separate domains, each reaching a diameter of up to 50 μm and containing 10^4–10^6 chains.

Molecular Architecture of the Condensed Domain. Despite the sharp increase in fluorophore-density variance throughout the transition, the integrated fluorescence intensity of the entire DNA-patterned area remained fixed (Figure S2A), implying redistribution of the labeled ends of the uniform brush into a nonuniform pattern in two dimensions. For a 3.5 kb chain, the free end can reach up to 1.2 μm from its anchoring site. Hence, fluorophore-rich regions (nucleation centers and dendrites) indicate colocalization of the labeled ends of nearby chains, whereas fluorophore-free regions (domain boundaries as well as gaps between proximal dendrites) indicate displacement of labeled ends away from their anchoring sites and toward the nearest bundle (Figure 1B).

Unperturbed, the resulting pattern remained stable for over a week with no apparent deformation, allowing scanning by wet AFM to gain insight into the 3D structure. At low scanning resolution, the AFM and fluorescence microscopy images were nearly identical (Figure 1C), correlating the fluorophore distribution and DNA height. The measured height of the pattern was ~25 nm above the surface at the nucleation centers (Figure 1C) and only a few nanometers in the area surrounding them, indicating a fully collapsed state. Branching dendritic extensions had a typical width of 20–100 nm (Figures 1D and S3A), which under the assumption of the typical tight hexagonal packing of condensed DNA[35] indicates a few tens to hundreds of coaligned chains in a cross section. The continuous branching of a bundle during growth (Figure S3B) allows accessibility of the condensate to distantly anchored chains, apparently in order to minimize the condensate–solvent contact area under the constraints of chain immobilization and bending rigidity, similar to the case of toroids.[22]

Interestingly, the domain boundaries appeared thinner by AFM than by fluorescence (Figure 1C) and contained internal structural features that appeared in the AFM phase measurement (Figure S3C). Namely, while chain backbones resided at the boundaries and were observable by AFM, their labeled ends were depleted from the region. This portrays a molecular organization in which chains anchored at the boundaries assume an extended collapsed state perpendicular to the boundary axis, which therefore remains free of fluorophores (Figure 1B). Condensation of brushes with different chain lengths (960–5360 bp) (Figures 1E and S4A) revealed a linear relation between the fluorescence boundary width and the chain length (Figures 1F and S4B) with a slope that equals twice the DNA contour length. This value corresponds to the maximal distance by which labeled ends of adjacently anchored chains can be displaced away from one another, implying a fully extended collapsed state (Figure 1B). Mechanistically, the fact that a similar fluorescence-free boundary already appears at the perimeter of a nucleus and a growing domain (Figure 1A) indicates that growth occurs through the extended collapse of chains at the front of a condensate, yielding a propagating radial wave of orchestrated collapse. This chain reaction lasts until the radially growing domain reaches oppositely collapsing waves of adjacent domains, thus forming the domain boundary. In addition to the dependence of the domain boundary width on the chain length, a gradual reduction in domain size was observed as the chain length decreased (Figure S4A), with growth being completely blocked for 960 bp brushes. Furthermore, we found that the relative fluorescence at nuclei increased with chain length (Figure S4C), which is reasonable since the labeled ends of longer chains may reach a nucleus from a greater distance.

To obtain insight into the structural dynamics during brush collapse, the brush height was next monitored using total internal reflection fluorescence (TIRF) microscopy with an evanescence decay length of ~100 nm. In the osmotic regime, a precondensed 3.5 kb brush extends to a height of ~1 μm, which is well beyond the evanescent excitation length[31] and is therefore not measurable by TIRF. Condensation was triggered by adding a single aliquot of concentrated Spd solution (Figure 1G and Movie S2). In contrast to the constant epifluorescence signal, the overall TIRF signal kept increasing (Figure S2B), indicating that labeled ends were collapsing toward the surface while penetrating into the measurable depth of the evanescence wave. Notably, we did not detect any increase in TIRF in precondensed regions until they were in contact with a growing domain (Figure 1H), implying a sharp transition with chains roughly maintaining their extended conformation right until they condense. The sharp Spd pulse revealed a second growth mode in which a single dendritic extension rapidly propagates from a nucleation center until running into another condensed region, yielding a continuous ridge rather than a single nucleation spot (Figure 1G). This behavior is in contrast to the slow radially symmetric mode of dendritic growth observed with incremental increases in C_{Spd} (Figure 1A) and is apparently a result of the transient inhomogeneity in local C_{Spd}.

Critical Spd Concentration, Hysteresis, and Coexistence in Condensates. Given the elucidation of the structure, we next focused on characterizing the effect of Spd concentration, DNA density, and salt concentration on nucleation and growth. We used an array of patterned brushes with a small surface area (30 μm × 27 μm) for the purpose of monitoring the effect of brush parameters within the same field of view. In order to identify the critical Spd concentration (C^*_{Spd}), C_{Spd} was gradually increased by repeatedly exchanging the reservoir with a homogeneous Spd solution, thereby avoiding temporal overshoots in local C_{Spd}. A morphological transition was first observed at C^*_{Spd} = 61 μM, with a single nucleation growing into one condensed domain (Figure 2A).

dx.doi.org/10.1021/ja410960w | J. Am. Chem. Soc. 2014, 136, 4945–4953

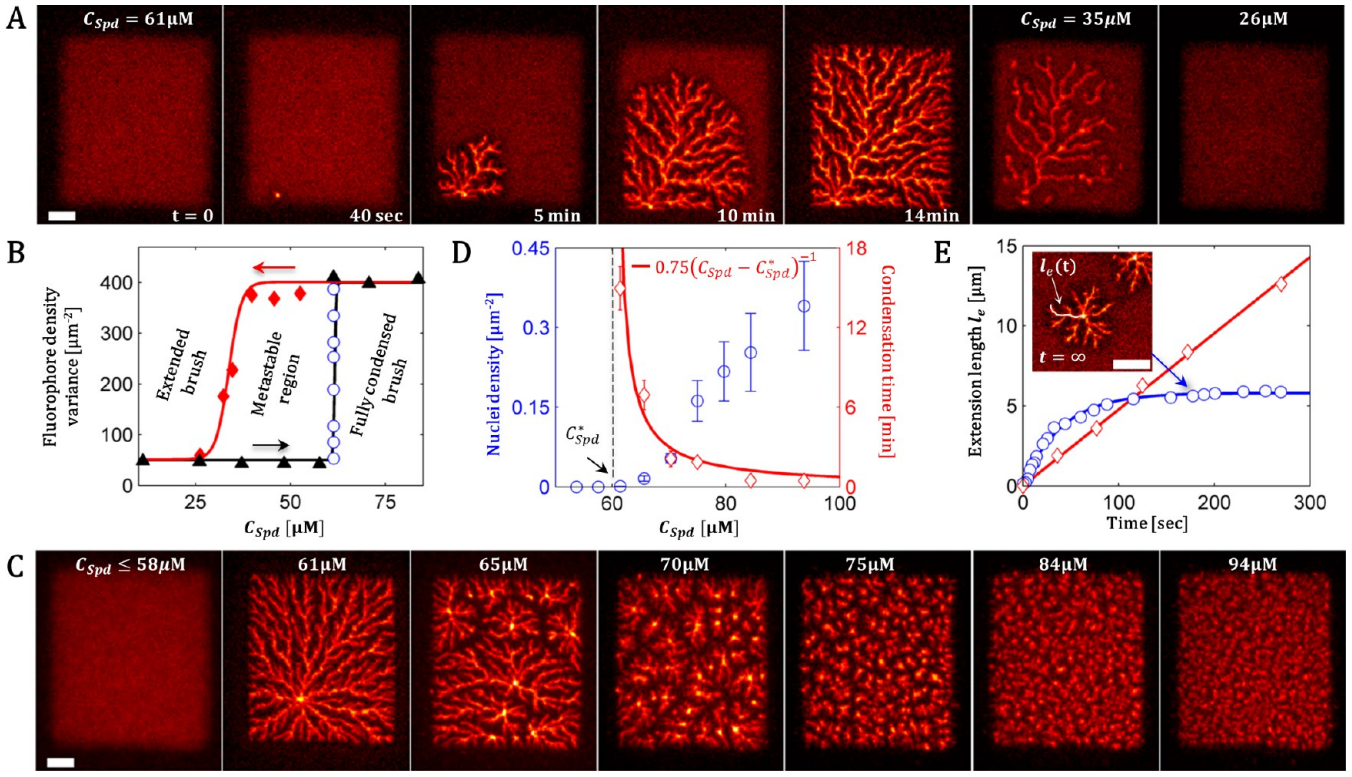

Figure 2. Reversibility, hysteresis, and coexistence. (A) Fluorescence images showing the growth of a nucleation into a single domain in a rectangular 3.5 kb DNA brush at a critical concentration of C^*_{Spd} = 61 μM (3 mM NaCl). Decreasing C_{Spd} induced decondensation back to a uniform brush via partially disassembled intermediates. (B) Plotting the change in fluorescence variance in response to increase and decrease in C_{spd} (black triangles and red diamonds respectively) shows hysteresis, metastability and full reversibility in a condensation-decondensation cycle. Blue circles represent time dependent variance during condensation. (C) Repeated condensation-decondensation cycles of the same brush at various C_{spd} were done, showing that (D) the density of nuclei increased with C_{Spd}, whereas the time from nucleation to complete growth decreased. (E) Coexistence between condensed and uncondensed phases (inset) was successfully stabilized by a pulsed overshoot of C_{Spd} to a supercritical local value that relaxed to a uniform subcritical value of $C_{Spd} \sim 50$ μM (within the metastable region), thereby inhibiting growth (blue). This behavior is in contrast to the constant growth rate at uniform supercritical C_{Spd} observed in (A) (red). Scale bars are 5 μm.

Once condensation was terminated, no further change was detected even when C_{Spd} was increased to 300 mM or decreased to 40 μM (much below C^*_{Spd}) during an incubation time of at least 1 h. Further reduction, however, initiated a reverse transition with a hysteretic nature (Figure 2B), beginning with deformation of the domain boundaries and thin dendritic bundles at 35 μM and continuing with complete disassembly of the main dendritic structures and nucleation centers at 26 μM (Figure 2). In both cases, the reverse transition occurred rapidly within less than 1 s. Notably, since C_{Spd} was kept uniform throughout the dilution experiment, the observed partial decondensation implies that nuclei and thick dendrites are more stable than thin dendrites that consist of fewer chains and involve less DNA-DNA interactions. Following decondensation, the fluorescence uniformity was restored to the precondensed state (Figure 2A), allowing successive condensation cycles.

Subjecting the same brush to C^*_{Spd} once again yielded a similar single domain condensate, yet this time the nucleation center emerged elsewhere (Figure 2C, 61 μM), indicating that nucleation occurs randomly within a uniform brush. Repeated cycles at higher C_{Spd} (65–94 μM) yielded an increasing number of nuclei (Figure 2C), smaller mean domain sizes due to the limited expansion area, and a shorter overall condensation time with a value inversely proportional to $C_{Spd} - C^*_{Spd}$ (Figure 2D). We note that when the internuclear distance was shorter than twice the contour length, the fluorescence intensity at the nucleation centers decreased (Figure S5 and Figure 2C at $C_{Spd} \geq 75$ μm), presumably because the overlapping nuclei competed for the same surrounding chains. The internuclear threshold distance of twice the contour length implies that the fully extended collapsed form is valid not only in dendritic growth (Figure 1A) and boundary formation (Figure 1F), but also during nucleation events. Interestingly, the overlapping nuclei did not coalesce in time, despite the tendency to maximize DNA–DNA interactions at the expense of DNA–solvent contact area. The stability of overlapping nuclei therefore indicates deep local free-energy minima, suggesting that the brush can be trapped within metastable coexistence (Figure 2B). To test that, we initiated condensation by transiently passing C^*_{Spd} via a Spd pulse, after which C_{Spd} slowly leveled off at a uniform concentration of 50 μM, in between C^*_{Spd} and the decondensation concentration. Consequently, the growth rate gradually decreased until stopping before domain boundaries were formed, yielding coexisting phases of condensed domains and extended brush that remained stable for hours (Figure 2E).

Increased Surface Density Promotes Nucleation and Growth. Since condensation requires the association of DNA segments, the brush density is expected to play an important role in modulating the nucleation and growth. To examine the role of density, we patterned an array of rectangular brushes of various densities ranging from 75 to 550 chains/μm^2 (Figure 3A, t = 0) and set C_{Spd} to slightly above C^*_{Spd} (65 μM) to initiate

dx.doi.org/10.1021/ja410960w | J. Am. Chem. Soc. 2014, 136, 4945–4953

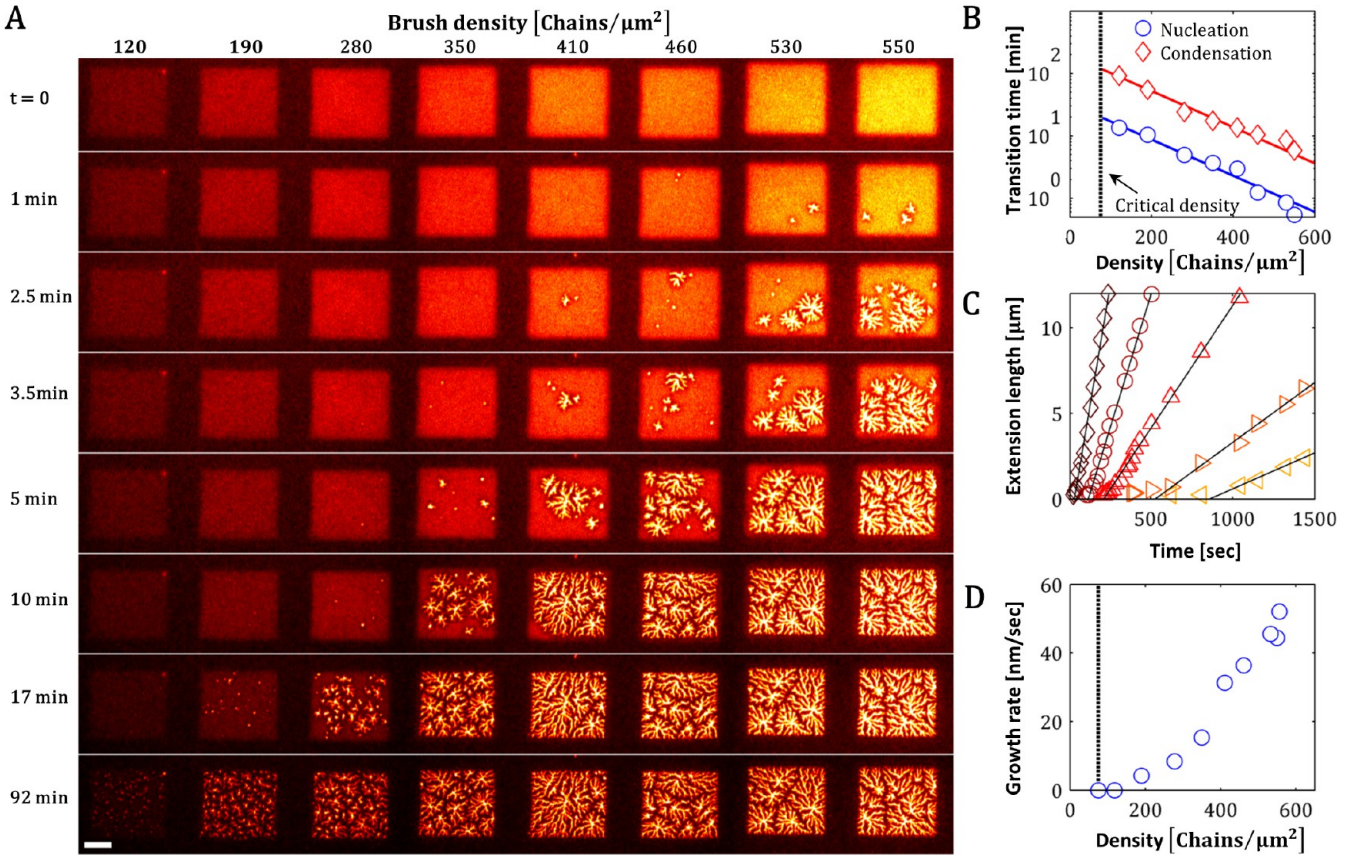

Figure 3. Enhancement of condensation with increasing DNA brush density. (A) Fluorescence images of an array of uniform brushes with various DNA densities, showing increased propensity for nucleation with increasing density (C_{NaCl} = 3 mM, C_{Spd} = 65 μM). The scale bar is 10 μm. (B) The characteristic times for nucleation initiation (blue) and overall condensation (red) decrease exponentially with increasing DNA density Dashed line corresponds to a surface density of 75 chains/μm^2, below which condensation did not take place (solid lines are exponential fits above the critical density). (C) Kinetics of linear growth of dendritic extensions (see the inset of Figure 2E) for various DNA densities (from left to right: 550, 410, 350, 280, and 190 chains/μm^2), with increasing lag time for nucleation. (D) Increase in growth rate of dendrites with brush density above the critical value (dashed line).

condensation. We found that decreasing the density led to (i) an exponential increase in the lag time for nucleation, measured as the time from Spd addition (Figure 3A,B) and (ii) a decrease in growth rate (Figure 3C,D), implying enhancement of nucleation and growth with increasing density. Fluorophore redistribution was completely inhibited at a density of ~75 chains/μm^2 even at C_{Spd} = 1 mM, thus setting a threshold for condensation. This inhibition could be an outcome of either the large distance between bound chains (~125 nm) or the relaxation in DNA conformation, which is coupled to the decrease in grafting density.[31]

To decouple conformation and density, we repeatedly condensed a dense brush at increasing NaCl concentration (C_{NaCl}), thus gradually relaxing the precondensed brush.[31] We found that C^*_{Spd} increases as a power law in C_{NaCl} with an exponent of 1.5 (Figure 4A). This is a known feature of condensation[36] that is attributed to the competition between counterions of different valence for the charged DNA[37] and is therefore unrelated to DNA conformation in a brush. Examining the morphology of the condensed brushes revealed a second salt-related effect: in contrast to the large domains formed at low salt concentrations ($C_{NaCl} \leq$ 10 mM; Figures 4B and S6), nucleation occurring at higher salt concentrations ($C_{NaCl} \geq$ 30 mM) exhibited negligible growth even when given ample time (Figure 4C). The resulting pattern was composed of multiple domains, each the size of a nucleation spot (Figure

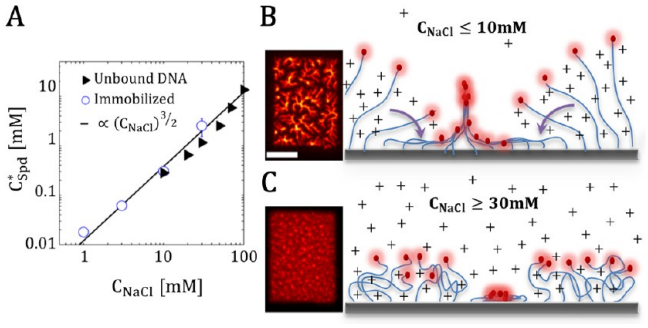

Figure 4. Effect of salt and chain conformation on brush condensation. (A) The critical Spd concentration increases with salt concentration (open circles, Figure S6) as a power law with exponent 1.5 and a coefficient α = 0.012, consistent with condensation of unbound DNA under dilute conditions (solid triangles; adapted from ref 36). (B) Large-scale condensates were formed only at very low salt concentrations (CNaCl ≤10 mM, see also Figure S6), where the precondensed brush assumes an extended conformation, suggesting a cascade of extended chain-to-chain collapse. The scale bar is 10 μm. (C) At $C_{NaCl} \geq$ 30 mM, growth was completely stopped even at $C_{Spd} \approx C^*_{Spd}$, and wide boundaries were not formed. The resulting condensed brush was composed solely of nuclei.

4C), independent of the value of $C_{Spd} - C^*_{Spd}$ (Figure 2C). Moreover, condensed domains formed at high salt concen-

dx.doi.org/10.1021/ja410960w | J. Am. Chem. Soc. 2014, 136, 4945−4953

trations lacked the wide boundary of fluorophore displacement, indicating that the surrounding chains of a nucleus did not collapse extendedly toward the nucleation center as was the case under low-salt conditions. Therefore, we conclude that an extended brush is an essential prerequisite for extended collapse and for the formation of large-scale condensates.

Growing Nanowires of Bundled DNA. Finally, we show that unraveling the molecular structure of the condensate combined with the ability to predetermine the number and location of nucleation events via C_{Spd} (Figure 2C) or surface density (Figure 3) enables us to control the morphology of a condensate, driving it to form nanowires of bundled DNA with predefined spatial patterning. For this purpose, 5.3 kb chains were patterned at intermediate density along a line 3 μm in width (Figure 5A). Since this width is thinner than twice the DNA contour length, it allows all of the chains within the cross section to coalign into a single point, in turn enabling the collapse of the entire brush into a single bundle. We note that exchanging the reservoir from high to low salt concentration (C_{NaCl} = 150 mM and 1 mM, respectively) prior to Spd addition led to substantial widening of the end-labeled line-shaped brush in approximately twice the DNA contour length (Figure 5B). This proves osmotic swelling of the brush, where the chains spread out in a fanlike structure to maximize the brush volume (Figure 5A, scheme).

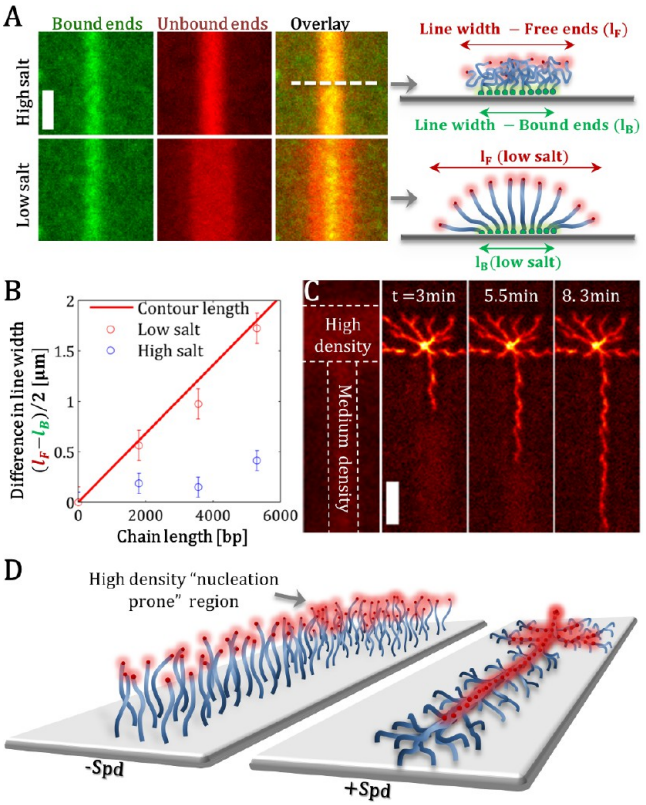

Figure 5. Directed brush collapse into nanowires. (A, B) 5.3 kb chains labeled at surface-bound and free ends were patterned along a line 3 μm in width. Prior to condensation, the bound chains were relaxed at high salt concentration and fully stretched at low salt concentration (C_{NaCl} = 150 mM and 1 mM, respectively),[31] forming a fanlike structure (scheme in A). (C) Slightly passing C^*_{Spd} initiated nucleation and growth in a highly dense "nucleation prone" region. Once the growing condensate reached the line-shaped brush, the chains collapsed into a single extension, thereby yielding a bundled nanowire with projecting tentacles, as shown schematically in (D). Scale bars are 5 μm.

Next to the line-shaped brush, we patterned a rectangular brush of maximal density as a nucleation prone site (Figure 5C). To minimize nucleation events, condensation was triggered at C_{Spd} slightly above C^*_{Spd}, which successfully yielded a single radially growing nucleation event in the designated rectangular area (Figure 5C). Once the interface was reached, the line-forming chains began collapsing toward the condensed rectangular brush, paving a restricted path for growth that led to the formation of a single bundled condensate (Figure 5C,D). On the basis of AFM measurements (Figure S3), we estimated the width of the nanowire cross section to be ~30 nm, yet a reduction in surface density would most likely allow the formation of much thinner wires.

DISCUSSION

Advantage of Exploring Condensation Using Brushes. In bulk solution experiments, the DNA concentration has been shown to modify the condensing agent and salt concentrations required for inducing condensation.[37] The local DNA density must therefore be decoupled from the overall DNA content in order to investigate the effect of density on condensation. Immobilizing the DNA solves this inherent problem in keeping a high local DNA concentration (~10 mg/mL) without affecting the bulk reservoir. It is important to note that the presence of a biocompatible surface did not alter the bulk reaction conditions, as implied by the identical C^*_{Spd} values for the brush and a typical solution experiment (Figure 4A).

Another advantage of the brush configuration is that the bulk reservoir can be replaced rapidly and uniformly without diluting the DNA and without causing overshoots in the local condensing agent and salt concentrations. Considering the hysteretic nature of the transition (Figure 2B), the latter is crucial for exploring and implementing condensation. Otherwise, the addition of small amounts of concentrated Spd creates transient inhomogeneity in Spd that induces rapid partial condensation at $C_{Spd} < C^*_{Spd}$ due to local entry into the metastable regime (Figure 2E). As a result, the sharp transition would appear continuous, requiring repeated additions of the condensing agent in order for complete condensation to occur.[37]

Hysteresis Is Due to a Hindered Forward Reaction. Hysteresis in the reversible condensation−decondensation cycle has been reported previously.[37,38] The cause was attributed to a kinetically blocked forward reaction (condensation) with a rapid reverse reaction (decondensation) , where the latter was suggested to represent the true thermodynamic equilibrium between condensed and uncondensed DNA.[37] A slow forward reaction is indeed supported by the long nucleation lag time observed here at $C_{Spd} \approx C^*_{Spd}$ (Figure 2D) or at low densities (Figure 3B,C). The kinetic barrier for condensation likely originates from the net electrostatic repulsion between negatively charged DNA segments at distances shorter than the Debye length, which inhibits attractive ion correlation interactions.[39] The enhancement of nucleation and growth by DNA density (Figure 3) appears to reduce this energetic barrier. A rapid reverse reaction is also supported by the data presented here as indicated by the instantaneous disassembly in response to small decrease in C_{spd} (Figure 2A). The fact that a lower C_{Spd} was required to decondense nuclei and thick bundles (26 μm) relative to thin dendrites (35 μm) (Figure 2A) indicates that condensed

dx.doi.org/10.1021/ja410960w | J. Am. Chem. Soc. 2014, 136, 4945−4953

structural elements with more chains are thermodynamically more stable, with nuclei being the most stable elements (Figure S5). Nevertheless, we found that overlapping nuclei (i.e., nuclei formed within a distance shorter than twice the contour length; Figure S5) did not coalesce into saturated nuclei with more DNA−DNA interactions and less DNA-solvent contact area (Figure 2C, $C_{Spd} \geq 75$ μm), implying a deep local minimum of the condensed form. Redissolution at increasing levels of condensing agent is a known feature in DNA condensation that involves charge reversal.[40,41] However, this transition, which typically occurs at ∼100 mM Spd for unbound DNA,[40] was not detected at up to C_{Spd} = 300 mM for an incubation time of 0.5 h.

Molecular Mechanisms for Growth. Depending on the chain configuration prior to Spd addition, we observed two types of nuclei. The first type are nongrowing nuclei formed either at high salt (Figure 4C) or low density (Figure 3C),where the precondensed chains are completely relaxed. AFM measurements under similar conditions indicated a transition into a fused globule by intra- and interchain nucleation.[34] Such structures are consistent with the absence of wide boundaries observed at high salt concentrations (Figure 4C). The second type are nuclei capable of growing into large-scale condensates. These are formed only at low salt and high density (Figures 3A and 4B), where the precondensed chains are extended. In such a configuration, intrachain nucleation is strongly inhibited,[38,42,43] and minimization of surface area at the expense of bending rigidity predicts interchain nucleation into a fused towerlike bundle.[44]

The likelihood of fused towers is supported by the increased height observed at the nucleation centers (Figure 1C) and furthermore by recalling the two identified growth modes. In the case of radially symmetric growth (Figure 1A), a towerlike nucleus produces a newly available volume around it, toward which the surrounding brush is attracted because of the reduction in osmotic pressure. The resulting fanlike structure (Figure 5A) allows the continuous approach of the surrounding chains toward the condensate while maintaining their extended conformation (Scheme 1A). This mechanism may explain the ordered growth patterns and the linear growth rate (Figure 3C) and, more importantly, the growth inhibition under high-salt conditions. In the absence of osmotic pressure, the relaxed surrounding chains are not driven toward the condensate, and hence, the kinetic barrier for growth, which is present also in condensation of DNA in solution,[45] is sustained, indicating that a dense DNA brush dramatically facilitates growth. The second mode, where we observed asymmetric growth of a single rapidly growing extension (Figure 1G) could be the result of a tower-shaped nucleus collapsing extendedly in an arbitrary direction. In such a case, nearby chains appear to align along the collapsed tower-shaped nucleus in a domino-like manner, yielding a single, rapidly growing bundle (Scheme 1B).

Effect of Chain Length on Condensation of a Brush. In addition to the effect of the chain length (960−5300 bp) on the domain boundary width, which provided insight into the chain configuration in condensate (Figures 1E,F and S4), we identified ∼1 kb as the minimal length above which dendrites grow (Figures 1E and S4). This is reasonable considering the ∼150 bp persistence length, which resists bending. The fact that new nucleation events can emerge but dendrites of existing nuclei do not grow presumably stems from nuclei gathering more chains (Figure S4C), making them more stable than dendrites (Figure 2A). For chains shorter than 500 bp, we could not detect condensed patterns because of resolution limitations. We speculate that in short DNA brushes nucleation may also be inhibited because of chain rigidity. At the other extremity, the fact that dendritic assemblies formed in DNA brushes of up to 35 persistence lengths, well within the polymeric regime, suggests that brush condensation is likely to occur for much longer chains provided the brush is sufficiently dense to assume an extended conformation. The combination of decreasing chain length and increasing density leads to the formation of smaller domains (Figure S4), suggesting a higher nucleation rate since nuclei have less available spreading area. We speculate that this is mostly a density-dependent effect, since the nucleation rate is strongly enhanced with increasing surface density (Figure 3). Nevertheless, further work is required to fully understand the effect of chain length on domain size.

Scheme 1. Proposed Scheme of Condensation Growth Modes[a]

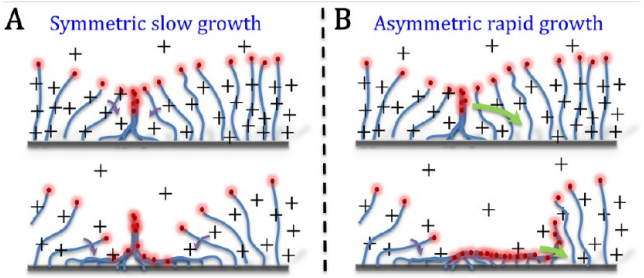

[a]Extended precondensed chains near a boundary are organized in a fanlike structure in order to decrease the osmotic pressure of the brush neutralizing counterions (Figure 4A). Similar organization is expected at the periphery of a newly available volume formed by nucleation. Two growth modes were observed: (A) Slow, radially symmetric growth (Figure 1A). Under this mode, the first layer of chains of the fanlike structured brush surrounding the nucleus collapses toward it, allowing the collapse of the next layer, hence forming a propagating radial wave of continuous chain-to-chain collapse. (B) Asymmetric growth via a single rapidly growing extension (Figure 1G). In this case, it is the tower-shaped nucleus that seems to collapse toward an arbitrary direction, allowing rapid coalignment of the nearby chains in a continuous domino-like cascade. Chains beyond the course of this rapidly growing extension keep condensing via the slow radially symmetric growth mode.

Implications of Controlled Condensation in Vivo. Bacterial DNA is known to be packaged into a subcellular compartment with high-order architecture[46,47] that is maintained by structurally restricted loops and cross-links stabilized by DNA-associating proteins.[48,49] Upon stress conditions, this organization undergoes a phase transition into a highly compacted and ordered state, primarily through the expression of nonspecific DNA binding proteins.[13] As a result, DNA transactions are significantly inhibited, supposedly because of inaccessibility of active protein machinery to DNA sequences. Nevertheless, a protein-independent mechanism for condensation was also observed, either at long starvation times or upon intervention through gene knockouts. In both cases, condensation was shown to be promoted primarily by polyamines.[13] The resulting condensed structures exhibit unique morphologies,[2,13] apparently as an outcome of different local structural restrictions applied on the DNA by scaffold proteins. Taking these results together, we hypothesize that the dependence of nucleation and growth on DNA density,

dx.doi.org/10.1021/ja410960w | J. Am. Chem. Soc. 2014, 136, 4945−4953

combined with the ability of cells to shape their local DNA density via DNA scaffolding proteins, may act as a cellular mechanism for regulating DNA transactions in three dimensions by selectively inducing condensation in well-defined chromosomal territories. Furthermore, oscillation in the polyamine concentration, which was observed in cells along their life cycle,[50,51] could in turn be a cellular way to stabilize coexistence due to the hysteretic nature of condensation, thus selectively silencing dense regions while allowing less dense regions to stay accessible and functional.

Prospective Uses of Controlled Condensation of Dense DNA. The Spd-induced transition in a brush and the ability to spatially shape the condensed morphology, as demonstrated here, enable the use of condensed DNA as a novel biomaterial in which nanowires can be easily formed in any desirable spatial pattern using light-directed patterning on a biochip. The reduction in dimensionality in the 2D distribution of the unbound ends could in turn be used to bind secondary molecules to the free ends with nanometric accuracy by simple chemical modifications. The structural control shown here could also open possibilities for investigating biochemical activity in condensed DNA, adding a new means to regulate biochemistry in cell-free gene expression systems. Condensed and uncondensed brushes are likely to exhibit significantly different gene expression patterns as the machinery interacting with DNA responds to the collective conformational changes.[28] It is likely that gene brushes could be switched on and off selectively, acting in coexistence between states, solely on the basis of their local density and in response to an externally triggered condensation. We note that the use of polyamines with higher valence, such as spermine^{4+}, which may reduce C^*_{Spd} by nearly 2 orders of magnitude,[36] may allow work under more "physiological" salt conditions.

■ ASSOCIATED CONTENT

Supporting Information

Methodology of biochip fabrication and DNA brush preparation and imaging; movies (AVI) showing the changes in epifluorescence and TIRF signals of the DNA brush in response to Spd addition; Spd addition modes; mass fractal dimension analysis of DNA domains; epifluorescence and TIRF quantification during brush condensation; and additional AFM images and additional fluorescence images of condensation for various chain lengths and salt conditions. This material is available free of charge via the Internet at http://pubs.acs.org.

■ AUTHOR INFORMATION

Corresponding Author

Roy.bar-ziv@weizmann.ac.il; brahadan@gmail.com.

Notes

The authors declare no competing financial interest.

■ ACKNOWLEDGMENTS

The authors thank Irit Goldian and Nir Kampf for support with AFM imaging. The authors also thank Shirley S. Daube, Yahel Atsmon, Eyal Karzbrun, Sam Safran, and especially Philip A. Pincus for fruitful discussions. This work was supported by the Israel Science Foundation, the Minerva Foundation, and the US–Israel Binational Foundation.

■ REFERENCES

(1) Bloomfield, V. A. *Biopolymers* **1991**, *31*, 1471–81.
(2) Livolant, F. *Phys. A* **1991**, *176*, 117–37.
(3) Spotheim-Maurizot, M.; Ruiz, S.; Sabattier, R.; Charlier, M. *Int. J. Radiat. Biol.* **1995**, *68*, 571–7.
(4) Wolf, S.; Frenkiel, D.; Arad, T.; Finkel, S.; Kolter, R.; Minsky, A. *Nature* **1999**, *400*, 83–5.
(5) Tsumoto, K.; Luckel, F.; Yoshikawa, K. *Biophys. Chem.* **2003**, *106*, 23–9.
(6) Krasnow, M.; Cozzarelli, N. *J. Biol. Chem.* **1982**, *257*, 2687–93.
(7) Luckel, F.; Kubo, K.; Tsumoto, K.; Yoshikawa, K. *FEBS Lett.* **2005**, *579*, 5119–22.
(8) Vijayanathan, V.; Thomas, T.; Thomas, T. J. *Biochemistry* **2002**, *41*, 14085–94.
(9) Estévez-Torres, A.; Baigl, D. *Soft Matter* **2011**, *7*, 6746–56.
(10) Estévez-Torres, A.; Crozatier, C.; Diguet, A.; Hara, T.; Saito, H.; Yoshikawa, K.; Baigl, D. *Proc. Natl. Acad. Sci. U.S.A.* **2009**, *106*, 12219–23.
(11) Tsuji, A.; Yoshikawa, K. *J. Am. Chem. Soc.* **2010**, *132*, 12464–71.
(12) Rizzo, P. J.; Jones, M.; Ray, S. M. *J. Protozool.* **1982**, *29*, 217–22.
(13) Frenkiel-Krispin, D.; Levin-Zaidman, S.; Shimoni, E.; Wolf, S. G.; Wachtel, E. J.; Arad, T.; Finkel, S. E.; Kolter, R.; Minsky, A. *EMBO J.* **2001**, *20*, 1184–91.
(14) Ames, B. N.; Dubin, D. T. *J. Biol. Chem.* **1960**, *235*, 769–75.
(15) Manning, G. S. *J. Chem. Phys.* **1969**, *51*, 924–33.
(16) Wilson, R. W.; Bloomfield, V. A. *Biochemistry* **1979**, *18*, 2192–6.
(17) Marquet, R.; Houssier, C. *J. Biomol. Struct. Dyn.* **1991**, *9*, 159–67.
(18) Pelta, J.; Durand, D.; Doucet, J.; Livolant, F. *Biophys. J.* **1996**, *71*, 48–63.
(19) Yoshikawa, K.; Takahashi, M.; Vasilevskaya, V. V.; Khokhlov, A. R. *Phys. Rev. Lett.* **1996**, *76*, 3029–31.
(20) Mel'nikov, S. M.; Sergeyev, V. G.; Yoshikawa, K. *J. Am. Chem. Soc.* **1995**, *117*, 2401–8.
(21) Gosule, L. C.; Schellman, J. A. *Nature* **1976**, *259*, 333–5.
(22) Ubbink, J.; Odijk, T. *Europhys. Lett.* **1996**, *33*, 353–8.
(23) Saminathan, M.; Thomas, T.; Shirahata, A.; Pillai, C. K. S.; Thomas, T. J. *Nucleic Acids Res.* **2002**, *30*, 3722–31.
(24) Wisecaver, J. H.; Hackett, J. D. *Annu. Rev. Microbiol.* **2011**, *65*, 369–87.
(25) Teif, V. B.; Bohinc, K. *Prog. Biophys. Mol. Biol.* **2011**, *105*, 208–22.
(26) Sarkar, T.; Vitoc, I.; Mukerji, I.; Hud, N. V. *Nucleic Acids Res.* **2007**, *35*, 951–61.
(27) Conwell, C. C.; Vilfan, I. D.; Hud, N. V. *Proc. Natl. Acad. Sci. U.S.A.* **2003**, *100*, 9296–301.
(28) Daube, S. S.; Bracha, D.; Buxboim, A.; Bar-Ziv, R. H. *Proc. Natl. Acad. Sci. U.S.A.* **2010**, *107*, 2836–41.
(29) Buxboim, A.; Daube, S. S.; Bar-Ziv, R. H. *Mol. Syst. Biol.* **2008**, *4*, No. 181.
(30) Buxboim, A.; Bar-Dagan, M.; Frydman, V.; Zbaida, D.; Morpurgo, M.; Bar-Ziv, R. H. *Small* **2007**, *3*, 500–10.
(31) Bracha, D.; Karzbrun, E.; Shemer, G.; Pincus, P. A.; Bar-Ziv, R. H. *Proc. Natl. Acad. Sci. U.S.A.* **2013**, *110*, 4534–8.
(32) Shemer, G.; Atsmon, Y.; Karzbrun, E.; Bar-Ziv, R. H. *J. Am. Chem. Soc.* **2012**, *134*, 3954–6.
(33) Bar, M.; Bar-Ziv, R. H. *Nano Lett.* **2009**, *9*, 4462–6.
(34) Kobayashi, K.; Tateishi-Karimata, H.; Tsutsui, K.; Wada, Y.; Sugimoto, N. *Chem. Lett.* **2011**, *40*, 855–7.
(35) Hud, N. V; Downing, K. H. *Proc. Natl. Acad. Sci. U.S.A.* **2001**, *98*, 14925–30.
(36) Korolev, N.; Berezhnoy, N. V.; Eom, K. D.; Tam, J. P.; Nordenskiöld, L. *Nucleic Acids Res.* **2009**, *37*, 7137–50.
(37) Widom, J.; Baldwin, R. L. *J. Mol. Biol.* **1980**, *144*, 431–53.
(38) Besteman, K.; Hage, S.; Dekker, N. H.; Lemay, S. G. *Phys. Rev. Lett.* **2007**, *98*, No. 058103.
(39) Bloomfield, V. A. *Biopolymers* **1997**, *44*, 269–82.
(40) Pelta, J.; Livolant, F.; Sikorav, J. L. *J. Biol. Chem.* **1996**, *271*, 5656–62.
(41) Besteman, K.; Van Eijk, K.; Lemay, S. G. *Nat. Phys.* **2007**, *3*, 641–44.

(42) Baumann, C. G.; Bloomfield, V. A.; Smith, S. B.; Bustamante, C.; Wang, M. D.; Block, S. M. *Biophys. J.* **2000**, *78*, 1965−78.
(43) Van den Broek, B.; Noom, M. C.; van Mameren, J.; Battle, C.; Mackintosh, F. C.; Wuite, G. J. L. *Biophys. J.* **2010**, *98*, 1902−10.
(44) Bright, J. N.; Williams, D. R. M. *Europhys. Lett.* **1999**, *45*, 321−6.
(45) Porschke, D. *Biochemistry* **1984**, *23*, 4821−8.
(46) Mercier, R.; Petit, M.-A.; Schbath, S.; Robin, S.; El Karoui, M.; Boccard, F.; Espéli, O. *Cell* **2008**, *135*, 475−85.
(47) Espeli, O.; Mercier, R.; Boccard, F. *Mol. Microbiol.* **2008**, *68*, 1418−27.
(48) Postow, L.; Hardy, C. D.; Arsuaga, J.; Cozzarelli, N. R. *Gene Dev.* **2004**, *18*, 1766−79.
(49) Browning, D. F.; Grainger, D. C.; Busby, S. J. *Curr. Opin. Microbiol.* **2010**, *13*, 773−80.
(50) Mei, Y. H.; Wilson, T.; Khan, A. U. *Quím. Nov.* **1993**, *16*, 337−42.
(51) Tabor, C. W.; Tabor, H. *Annu. Rev. Biochem.* **1976**, *45*, 285−306.